Fuel Effects on Advanced Compression Ignition Load Limits

Author, co-author (Do NOT enter this information. It will be pulled from participant tab in MyTechZone)

Affiliation (Do NOT enter this information. It will be pulled from participant tab in MyTechZone)

Abstract

In order to maximize the efficiency of light-duty gasoline engines, the Co-Optimization of Fuels and Engines (Co-Optima) initiative from the U.S. Department of Energy is investigating multi-mode combustion strategies. Multi-mode combustion can be describe as using conventional spark-ignited combustion at high loads, and at the part-load operating conditions, various advanced compression ignition (ACI) strategies are being investigated to increase efficiency. Of particular interest to the Co-Optima initiative is the extent to which optimal fuel properties and compositions can enable higher efficiency ACI combustion over larger portions of the operating map. Extending the speed-load range of these ACI modes can enable greater part-load efficiency improvements for multi-mode combustion strategies. In this manuscript, we investigate fuel effects for six different fuels, including four with a research octane number (RON) of 98 and differing fuel chemistries, iso-octane, and a market representative E10 fuel, on the load limits for two different ACI strategies: spark-assisted compression ignition (SACI) and partial fuel stratification-gasoline compression ignition (PFS-GCI) operation. Experimental results show that limits to intake boosting limit high load operation for most fuels, but high smoke emissions for high particulate matter index (PMI) fuels under SACI conditions could also be a limitation. Contrastingly, low load is limited by combustion efficiency, but these effects have more pronounced variation with fuel chemistry for PFS-GCI than with SACI. Additional, distinct effects affecting autoignition timing and peak heat release at higher speeds were identified for fuels having different low temperature heat release (LTHR) propensities for both ACI modes.

Introduction

Within the U.S. Department of Energy, the Co-Optimization of Fuels and Engines (Co-Optima) initiative is working to increase engine efficiency, and to identify areas where fuel properties and compositions enable that higher efficiency. Recent work has suggested the gains by utilizing fuels with high RON and octane sensitivity could be up to 10% with boosted spark ignited (SI) engines [1]. While this represents a substantial improvement in efficiency, the use of advanced compression ignition (ACI) combustion under part-load conditions as part of a larger multi-mode combustion strategy could enable further efficiency improvements or could achieve the 10% improvement with less costly fuel property improvements.

Using ACI combustion modes at part-load operation has several fundamental thermodynamic advantages compared to traditional spark-ignited (SI) engines. First, ACI strategies are typically unthrottled, which drastically reduces the level of pumping work and the associated fuel economy penalty at part-load conditions relative to SI operation [2]. A second advantage is the use of dilute, fuel-lean operation. This reduces peak combustion temperatures and heat transfer, and improves the ratio of specific heats, further improving thermal efficiency [3–5]. These fundamental improvements over SI operation lead to an estimated efficiency benefit on the order of 15% in simulations [6], and work within the Co-Optima initiative has demonstrated that relative efficiency benefit of ACI can be as high as 19% at part load operation [7]. The limited operating range for ACI modes requires they be paired with traditional spark-ignited operation to maintain the power density benefits of modern engines.

Dempsey et al. provide an overview of a spectrum of different ACI operating strategies based on the degree of charge stratification for gasoline compression ignition strategies [8]. Homogeneous charge compression ignition (HCCI) is one extreme in this spectrum and applies when the fuel and air are completely premixed. However, HCCI experiences excessive pressure rise rates and combustion noise at high load, and at low load it experiences low combustion efficiency and high cycle-to-cycle variability [9,10]. Dempsey et al. [8] described that introducing varying degrees of fuel-air stratification can be introduced to allow control of the combustion event, which can collectively be called partially premixed compression ignition (PPCI). When PPCI is mostly well-mixed and the fuel-air stratification is minimal, this can be referred to as partial fuel stratification (PFS), and when the majority of the fuel and air are stratified, this can be referred to as heavy fuel stratification (HFS). There is a tradeoff between the emissions and controllability, where PFS has lower soot and NOx emissions and HFS exhibits better

controllability. In this investigation, the PFS subset of PPCI is investigated because the low NOx and soot emissions potential of this combustion mode is desirable to simplify the emissions control system for multi-mode operation.

An alternative ACI strategy being considered for SI multi-mode combustion systems is spark-assisted compression ignition (SACI) [11–13]. In this strategy, a deflagration event initiated by the spark plug compresses the unburned air and fuel to the point of autoignition. This provides control of the autoignition event timing, reducing the peak pressure rise rate and combustion noise, and allows for compression ignition combustion to be achieved in the lower compression ratio engines typically associated with SI combustion. A form of SACI combustion has been commercialized by Mazda in the Skyactiv X [14], and as a result, this form of ACI combustion is being investigated here.

The Co-Optima initiative is interested in identifying fuel properties or compositions that can enable these ACI operating strategies for multi-mode engines. Co-Optima has thoroughly identified and quantified fuel properties that are beneficial for SI combustion [15]. Since multi-mode engines continue to rely on SI combustion at high loads, it is important to preserve the fuel properties that enable high efficiency in SI engines, which are important to resisting end gas knock. Within this constraint, recent research has demonstrated that fuel chemistry can significantly alter the required ACI operating parameters [16,17]. One study by Szybist et al. [16] found that for HCCI, which utilized very high temperatures at intake valve closing (IVC), aromatic fuels required significantly greater intake temperature to achieve similar combustion phasing to other fuel chemistries with matched RON and octane sensitivity. A follow-on investigation of SACI and PFS-gasoline compression ignition (PFS-GCI) [18] found that many of the fuel-specific trends from [16] were not repeated and concluded that the effects of fuel chemistry vary depending on the ACI mode. In some respects, this is not surprising because it is well-known that the relative autoignition propensity can change between operating conditions [15,19,20], and these changes are the basis for the octane index [21,22].

The different fuel property effects between HCCI combustion by Szybist et al. [16] compared to the findings of Powell et al. [18] under SACI and PFS-GCI conditions makes it clear that there are limitations to lumping all ACI combustion modes into the same category. In this follow-on study to these prior investigations [16,18], the load limits of the SACI and PFS-GCI forms of ACI combustion are explored. Then, an in-depth analysis of the combined effects of fuel chemistry and engine speed on the load limits for SACI and PFS-GCI is conducted.

Experimental Setup and Procedure

Engine

The multi-mode engine used in this set of experiments is based on a modified Ricardo Hydra single-cylinder engine. It is equipped with a custom cylinder head having a centrally-mounted direct fuel injector, 4-valves per cylinder, and cam phasers enabling flexible cam timing. The intake and exhaust cams each have 60 degrees of cam timing authority, depicted in Figure 1 with a nominal cylinder pressure trace, enabling up to 80 degrees of negative valve overlap for high residual trapping. The engine is also designed with a 12.5:1 geometric compression ratio. The combination of these two features enable multi-mode operation with the engine. Additional details on the bore, stroke and other engine geometry are provided in Table 1.

Table 1. Engine Geometry.

Displaced volume	550 cc
Bore	86.0 mm
Stroke	94.6 mm
Connecting Rod	145.5 mm
Compression ratio	12.5:1
Number of Valves	4
Intake and Exhaust Valve Timing	Variable with 60°CA control authority, see Figure 1 for timing
Fuel Injector	DI solenoid-type with 8 holes and symmetric 60° included angle

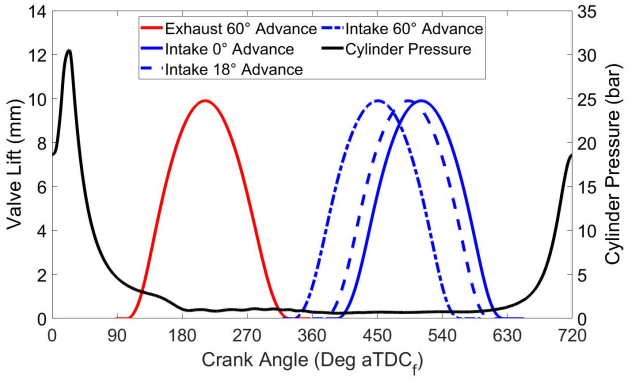

Figure 1. Valve lift profiles for cam timings used in this set of experiments.

This engine setup is identical to one used in a prior investigation, and is discussed in greater depth in [18]. However, a brief overview of the relevant experimental setup is given here.

Air to the engine is supplied by passing compressed and dried air with a relative humidity of less than 5% through a mass flow controller (Alicat PCR3) and through a downstream inline electric heater. This provides direct control of the airflow regardless of the intake boosting level. While the intake can operate boosted, the exhaust is left at atmospheric conditions, which is more representative of conditions present in a supercharged engine. Compared to operation with higher backpressure, this will reduce the total trapped residuals for ACI operation, shifting the operability limits to higher loads. Measurements of exhaust equivalence ratio are provided by an EGR 5230 meter and a pressure-compensated wideband oxygen sensor.

Fuel at a regulated pressure of 100 bar is supplied to the engine by means of a pressurized 1.5 gallon fuel accumulator. Fuel flow measurements are taken with an inline-mounted Coriolis-type meter (MicroMotion CMF010). The fuel is sent to an 8-hole Bosch solenoid injector capable of injecting multiple times per cycle. Further details of the injector are provided in Table 1.

For SACI operation, the spark is supplied by the stock ignition coil from a 2.0L GM LNF engine using a spark dwell of 3ms. An NGK Iridium spark plug (heat range 7) is used in this investigation. It is clocked to avoid the ground strap from interfering with the spray from the adjacent fuel injector.

Emissions measurements of exhaust hydrocarbons, CO, CO_2, O_2, and NO_x are provided by a standard 5-gas bench using California Analytical Instruments analyzers (Models 700-HFID, 700-HCLD, and 600-NDIR). These exhaust emissions measurements also provided backup equivalence ratio measurements and combustion efficiencies, which are calculated by the method outlined by Heywood [3]. Exhaust smoke level measurements are taken with an AVL 415s smoke meter.

Engine control and data acquisition is managed by a National Instruments Powertrain Control platform. Measurements of cylinder pressure, intake pressure, spark discharge command, and fuel injector current are measured at 0.1°CA intervals over 300 consecutive cycles.

Combustion analysis is performed using a custom-developed Matlab script. Cylinder pressure is pegged to the intake pressure over a ±5°CA interval at 180°CA bTDC firing. The intake manifold and cylinder pressures are measured using Kistler 4049A piezoresistive and Kistler 6125C piezoelectric pressure sensors, respectively. Heat release is computed on a first-law basis according to the method outlined by Heywood [3], and convection coefficients by the Woschni method [23] for SACI, and the modified Woschni method developed by Chang et al. [4] for PFS-GCI. The residual fraction is computed by taking an average of the State [24], the Yun and Mirsky [25], and Fitzgerald [26] methods.

Operating Methodology

The operating procedure and load limits will be discussed in detail in this section. It should be noted that the operating conditions were chosen to investigate differences in load limits due to fuel chemistry with a consistent methodology. As such, the operating conditions were not individually optimized for each fuel, and the control parameter space to identify the absolute maximum operability of each ACI mode was not fully exhausted. For example, the use of cooled exhaust gas recirculation, variable intake temperatures, and different injection strategies may enable some increases in operating limits for both modes, but this level of optimization is outside the scope of the present work.

Load Limit Criteria

The criteria for determining the low and high load limits are identical for SACI and PFS-GCI. The high load limit is reached whenever one of the following conditions is reached: (i) the peak pressure rise rate (PPRR) reaches or exceeds 7 bar/°CA, (ii) when intake pressure reaches 200 kPa absolute, (iii) when the filter smoke number, or FSN, reaches a value of one. Similarly, the light load limit is reached whenever: (i) the combustion efficiency drops to 92.5%, (ii) when the coefficient of variation (COV) of indicated mean effective pressure (IMEP) reaches 4%. The limitations utilized in this investigation are beyond what would typically be acceptable for a production engine. However, it was desirable to extend these criteria beyond the acceptable production limits as an acknowledgement that further optimization of the operating conditions may be possible, and to accentuate fuel-specific differences.

Spark-Assisted Compression Ignition Operation

For SACI operation, the intake temperature is set to 70°C, while the intake and exhaust cam advances are 0° and 60°, respectively. The resulting cam lift profiles are shown in Figure 1. SACI is being operated globally lean in this investigation, with a fixed global equivalence ratio (φ) of 0.5. However, this necessitates fuel-stratified operation with a locally higher concentration of fuel near the spark plug to enable reliable deflagration [27]. As a result, the fuel injection events are split into an early event at 280°CA $bTDC_f$ and a second event much closer to the TDC. The timing of the second injection is variable, but it is separated from the spark event by a fixed timing of 4°CA with the intent of maintaining a constant stratification level over a range of combustion phasing. Since the spark is the combustion trigger for SACI combustion, retarding both events results in later combustion, this approach is summarized visually in Figure 2 below.

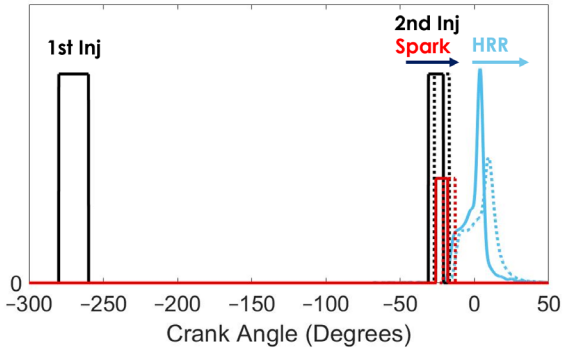

Figure 2. SACI spark and fuel injection strategy, also the effects of retarding the 2nd injection and spark events on combustion. Adapted from [18].

The injection split for high load is 75%/25% of the total commanded injection duration at 100 bar fuel pressure between the primary and second injections. This is changed to a split of 70%/30% of the commanded injection duration and a fuel pressure of 80 bar at light load to avoid having an injection event shorter than a commanded 0.25ms, which was observed to be the minimum injection duration for repeatable operation.

To determine the high load limit, the spark and 2nd injection timing were retarded in unison and fuel and air mass are increased at a constant equivalence ratio until the criteria for the high load limit were satisfied. The light load limit is encountered at the advanced combustion phasing limit (50% burn timing, CA50) of -8°CA $aTDC_f$. This phasing was held constant while decreasing the fuel and air at a constant equivalence ratio until the light load limitations were encountered. CA50 combustion phasing earlier than -8°CA $aTDC_f$ results in reduced efficiency.

Partial Fuel Stratification Gasoline Compression Ignition Operation

For PFS-GCI, the intake temperature is set to 165°C, while ϕ is fixed at 0.33. The operating methodology for PFS-GCI differs from SACI in that stratification is used to create a reactivity gradient that affects the autoignition timing. This means retarding injection timing to increase fuel stratification will advance combustion. In order to develop fuel stratification, one injection is made early in the cycle at 280°CA $bTDC_f$, while the second has a variable timing but occurs closer at 110°CA $bTDC_f$ or later. A visual representation of this

methodology is shown in Figure 3. A fixed injection split of 70%/30% of the total commanded injection duration at a pressure of 100 bar is used.

While the spark timing for SACI controls the peak pressure rise rate, PFS-GCI depends on modulation of the effective compression ratio through changes to the intake valve closing (IVC) timing. To determine the high load limit, the injection is set to the earliest timing considered, 110°CA bTDC$_f$, and the load is increased by increasing air and fuel at a constant equivalence ratio while IVC is simultaneously retarded to control the maximum pressure rise rate. This process is repeated until the high load limit criteria are met, which in all cases was the maximum intake manifold pressure limitation for PFS operation. A 2-step process is used to approach the light-load limit for PFS. First, fuel and air are decreased while advancing the IVC timing to its advance limit of 60° at a constant injection timing of 110°CA bTDC$_f$. Then, to enable further reductions in load, fuel and air are reduced at a constant φ while the 2nd injection timing is retarded to increase fuel stratification. This is repeated until one of the light load limitations is encountered. Intake cam timing advances used are shown in Figure 1.

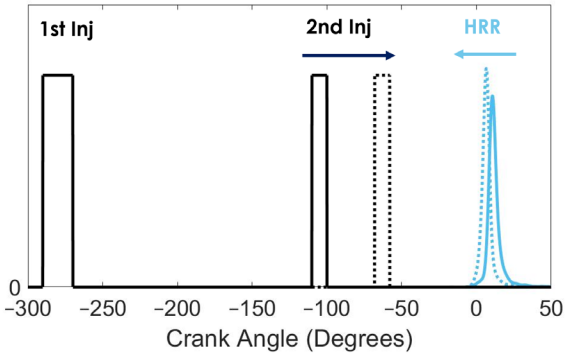

Figure 3. PFS-GCI fuel injection strategy and the effect of retarding the 2nd injection timing on combustion. Adapted from [18].

Fuels

A fuels matrix containing six fuels was used for this investigation. The matrix and associated fuel properties are shown in Table 2. Three of the six fuels share a common 98 octane RON rating with a nominal octane sensitivity of 10.5. These fuels are a subset of the core fuels used in the Co-Optima program [28]. While these three Co-Optima fuels have similar octane ratings, they have different chemical composition, and are high in aromatics, ethanol, and cycloalkanes, respectively.

Two additional fuels having nominal RON ratings of 98 were also included in the fuels matrix. While the 98 RON fuel with di-isobutylene is note one of the Co-Optima core fuels, it is similar to the olefinic core fuel in that it contains nominally 30% by volume of the olefin di-isobutylene. As a significant departure from the other 98 RON fuels, neat iso-octane is also used in this investigation. While it has a slightly higher RON rating than the other fuels, it has an octane sensitivity of zero. Iso-octane also boils at 99°C compared to the final boiling points (FBP) between 191 and 205°C for the other full-boiling range fuels. The most significant reason for the inclusion of iso-octane is its simpler and more established kinetics mechanisms, enabling easier validation of future modeling work.

The last fuel included in the fuels matrix is a market-representative E10 fuel (10% by volume of Ethanol) called RD5-87 available from Gage Products. It has lower RON rating of 92 compared to the other fuels, but it has been used in a number of prior investigations, so it can provide a useful comparison with the prior ACI work [18,29,30].

The fuels used in this set of experiments were also characterized by their particulate matter index, or PMI as outlined by Aikawa et al. [31]. PMI was developed as a composite fuel property so that the sooting tendency of a set of fuels could be ranked a priori regardless of the type of SI combustion system [31], and is a metric that was used extensively throughout the Co-Optima initiative [15]. Each fuel's PMI value is calculated using Equation 1, which is a function of the mass fraction (Wt_i), the double bond equivalent (DBE_i), and vapor pressure at 443K ($VP[443K]_i$) for each fuel component. The fuel PMI values for the Co-Optima Core fuels in Table 2 were computed by Fouts et al. [28], while the values for the di-isobutylene and RD5-87 fuels were calculated from detailed hydrocarbon analyses provided with the fuels.

$$PM\ Index = \sum_{i=1}^{n} \left(\frac{DBE_i + 1}{VP[443K]_i} \times Wt_i \right) \quad (1)$$

Table 2. Fuel Properties.

Property	Standard	Co-Optima Core Fuels			Di-isobutylene	Iso-Octane	RD5-87
		E30	Aromatic	Cyclo-alkane			
RON [-]	D2699	97.4	98.1	98.0	98.1	100.0	92.3
MON [-]	D2700	86.6	87.8	87.1	86.6	100.0	84.6
S_{octane} (RON – MON) [-]	calc	10.8	10.3	10.9	11.5	0.0	7.7
Saturates [vol%]	D1319	57.1	65	70.3	52.5	100.0	47.4
Aromatic [vol%]	D1319	8.1	30.8	18.1	13.5	0.0	23.8
Olefins [vol%]	D1319	5.0	4.2	1.5	33.1	0.0	5.9
Oxygenates [vol%]	D5589	30.6	0.0	0.0	0.0	0.0	9.1
Ethanol [vol%]	D5589	30.6	0.0	0.0	0.0	0.0	9.1
IBP [°C]	D86	35.7	35.7	35.7	30.6	99.3	40.4
T10 [°C]	D86	60.7	59.4	55.7	62.2	N/A	57.8
T50 [°C]	D86	74.3	108.1	87.4	102.8	N/A	101.3
T90 [°C]	D86	155.2	157.9	142.7	126.7	N/A	157.9
FBP [°C]	D86	204.1	204.4	203.5	191.1	99.3	205.0
RVP [psi]	D5191	7.66	7.17	8.00	8.71	--	--
LHV [$^{MJ}/_{kg}$]	D4809	38.17	42.95	43.21	43.85	44.31	41.93
Carbon [wt%]	D5291	74.78	87.22	87.08	85.88	84.28	82.67
Hydrogen [wt%]	D5291	13.79	13.12	13.24	14.39	15.91	13.66
Oxygen [wt%]	D5599	11.19	0.00	0.00	0.00	0.00	3.67
H:C	Calc	2.2	1.79	1.81	2.00	2.25	1.97
O:C	Calc	0.110	0.000	0.000	0.000	0.000	0.033
PMI	Calc	1.28	1.80	1.49	0.42	0.19	1.71
AFR_{stoich}	Calc	12.92	14.52	14.55	14.82	15.14	14.05
LHV for stoichiometric mixture per kilogram of air [$^{MJ}/_{kg\text{-}air}$]	Calc	2.95	2.96	2.97	2.96	2.93	2.99

Results

The results of this investigation are split into three separate sections. Fuel effects on SACI and PFS-GCI load limits are discussed in the first two sections. The third section investigates the change in heat release response of each fuel for SACI and PFS-GCI combustion modes.

Fuel Effects on SACI Load Limits

Figure 4 illustrates the format used to show the combined load limits on the left hand side, and the tracked load limit criteria on the right hand side. The load limit criteria are subdivieded into manifold absolute pressure (MAP) and FSN for high load, and coefficient of variation in net mean effective pressure (COVn) and combustion efficiency for low load. Figure 4presents the first three fuels that have the widest load range, 98 RON E30, di-isobutylene, and cycloalkane, while Figure 5 and Figure 6 add the other fuels to these same figures as a means of illustrating the differences. For the three fuels shown in Figure 4, their operating limits are almost overlapping. Intake boost was found to be the limiting factor for high load operation, while combusiton efficiency limited light load operation. However, the filter smoke emissions were found to vary widely between the fuels, with E30 producing the most smoke, and cycloalkane producing the least. While FSN does not limit operation for these fuels, it is noteworthy that the FSN values do not correlate with PMI, which is included in the fuel properties in Table 2. Specifically, the cycloalkane fuel has the highest fuel PMI and produces the lowest FSN values, and E30 has the lowest PMI and produces the highest FSN values at the two lowest engine speeds. Discussion of the FSN fuel trends will be revisited later in this section.

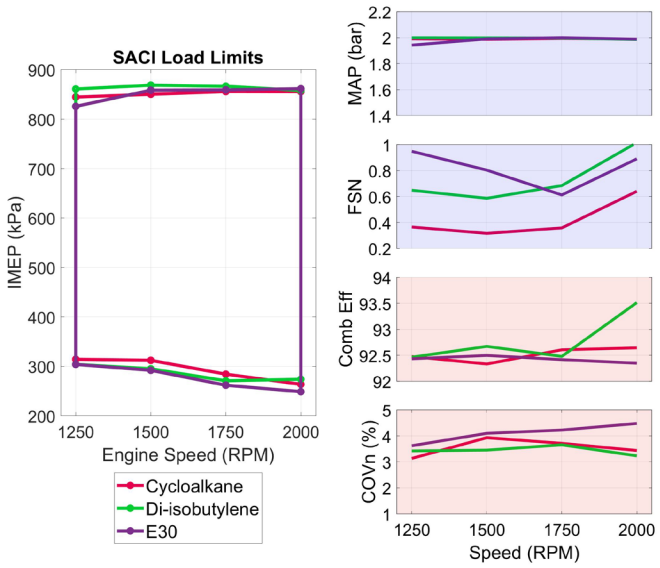

Figure 4. E30, di-isobutylene, and cycloalkane fuel load limits and load limit criteria.

Figure 5 adds the results of iso-octane to the results previously shown in Figure 4. It can be seen that iso-octane has a similar boost-limited high load limit to the E30, di-isobutylene, and cycloalkane fuels. However, iso-octane has a noticeably higher light load limit, due to having a lower light-load combustion efficiency. The cause for this isn't entirely clear, but could be associated with the lack of heavy boiling components causing fuel/air mixing differences, or due to the lower octane sensitivity of the iso-octane.

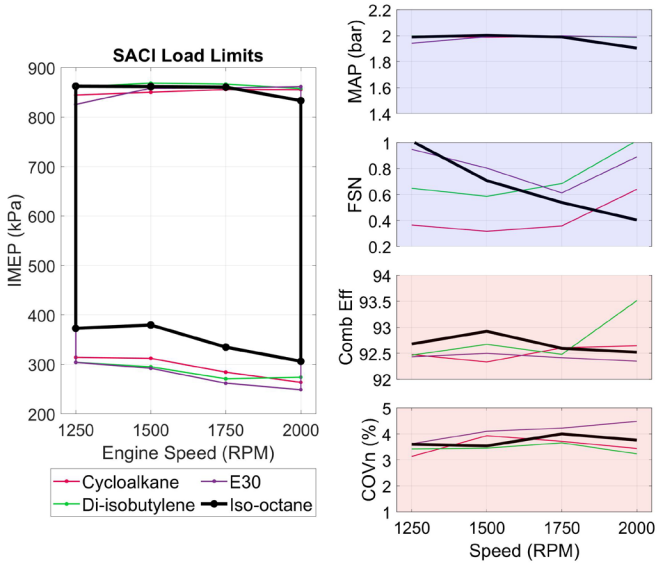

Figure 5. Iso-octane load limits and load limit criteria.

Figure 6 adds the SACI load limit data for the final two fuels: aromatic and RD5-87 fuels. The high load limits for these fuels are reduced relative to the four prior fuels. This is due to high smoke emissions, quantified by encountering the FSN limit. This result is consistent with the trends expected from PMI, with the aromatic having the highest value of 1.80, and RD5-87 having the second highest value of 1.71 PMI. At light load, it can be seen that RD5-87 is limited by combustion efficiency while the aromatic fuel is limited by high cycle-to-cycle variability. Both of these fuels have similar low load limits to the baseline set of fuels initially shown in Figure 4.

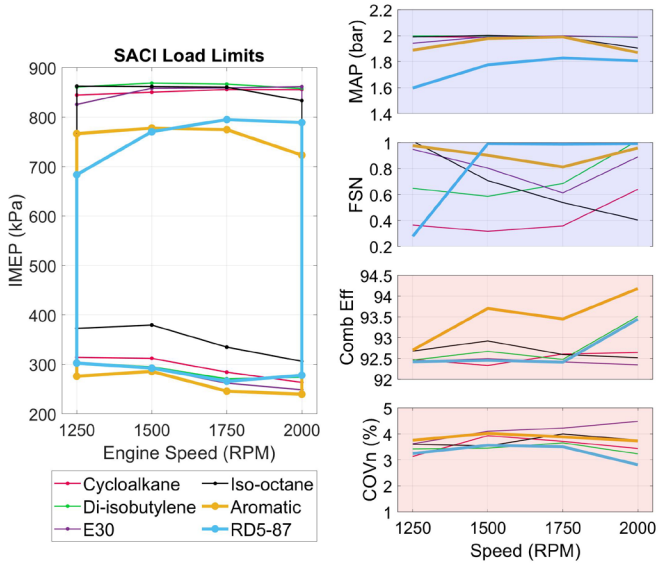

Figure 6. RD5-87 and aromatic fuel load limits and load limit criteria.

The smoke emissions for SACI operation, seen in Figure 7, were found to increase non-linearly with load. This effect is most pronounced at later injection timings and higher engine loads. There is also a general trend in decreasing maximum load with increasing fuel Particulate Matter Index (PMI), due to the fuels reaching the 1.0 FSN smoke limit. Given the non-linear nature of smoke emissions with SACI, limiting high load to 0.5 FSN would only reduce the load limit by roughly 50 kPa in most cases.

Hu et al. [27] experienced a similar non-linear increase in smoke emissions within the last 50-60 kPa of the high load limit for fuel-stratified SACI operation. Optical imaging of the fuel spray suggested the primary source of the smoke emissions was from the locally-fuel rich mixture near the spark plug, instead of pool fires resulting from fuel pooling on the piston. It is important to note that while dual injections were used by Hu et al. [27], a fixed-duration pilot (second) injection was used with a variable injection split. This differs from the fixed injection split approach used in the present investigation. A majority of the smoke emissions in the present investigation are likely due to the rapid increase in fuel stratification near the high load limit, but fuel pooling and consequential pool fires cannot be ruled out.

The results from Figure 7 provide some additional insight into the role of fuel PMI and smoke on the SACI high load limit. Given the PMI values for di-isobutylene (0.42 PMI) and E30 (PMI 1.28), it was not expected that these fuels would create higher levels of smoke than the cycloalkane fuel (1.49 PMI). This demonstrates a shortcoming in using PMI to predict smoke emissions. It is noteworthy, though, that the PMI framework was established for stoichiometric SI engines with both PFI and DI fueling where the intent was to fully premix the fuel and air prior to ignition. The shortcoming in PMI in this investigation is occurring with stratified charge combustion where there is significantly more opportunity for spray dynamics and differences in the distillation and vaporization processes to cause significant fuel-specific differences in the local equivalence ratio.

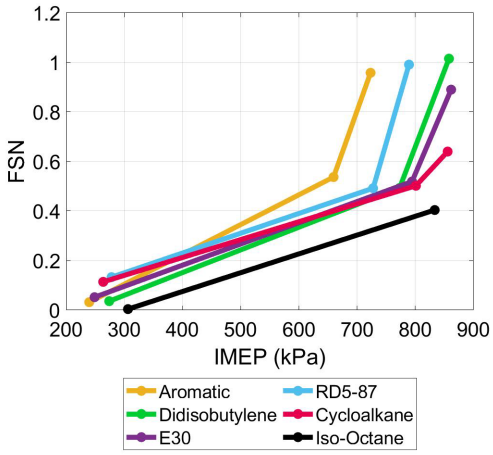

Figure 7. SACI smoke emissions versus engine load at 2000 RPM.

Fuel Effects on PFS-GCI Load Limits

The load limits for PFS operation are presented in a manner similar to SACI, where the results for subsets of fuels are added from Figure 8 through Figure 10. Figure 8 shows the di-isobutylene and aromatic fuels demonstrated similar levels of operability between 1250 to 2000 RPM. Both fuels were boost-limited at high load and showed similar light load levels at the combustion efficiency limit, although post-processing revealed that the aromatic fuel did not hit either of the light-load criteria at 1,250 rpm and could likely have been extended to even lower loads. The use of a variable IVC timing and effective compression ratio to compensate for individual fuel reactivity creates differences in mass trapping and ultimately high load limits at the maximum 200 kPa intake boosting pressure. PFS-GCI also differs from SACI because the smoke emissions, seen in Figure 8, are near-zero, even at high load. This is directly due to the timing of the 2nd injection at 110°CA $bTDC_f$ for high load being significantly earlier than for SACI, reducing fuel stratification level.

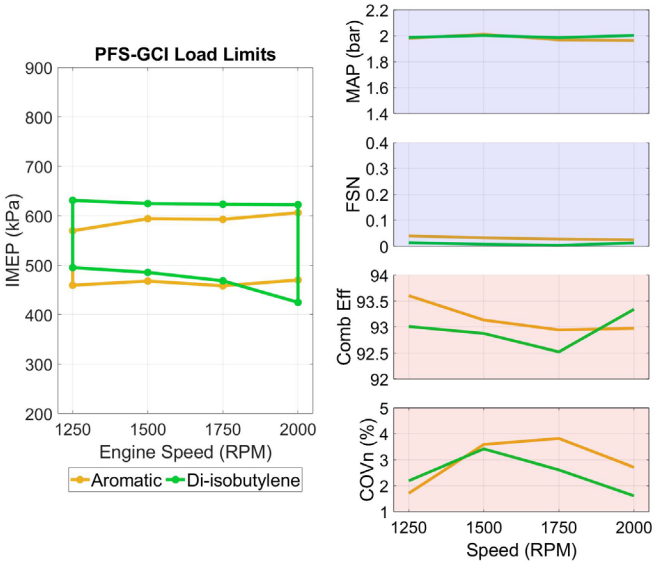

Figure 8. Di-isobutylene and aromatic fuel load limits and load limit criteria.

Figure 9 adds the load limits for E30 and RD5-87 and the overall reduction in operability relative to the aromatic and di-isobutylene fuels. The high load limit is still boost limited, seen in Figure 9, but the level doesn't shift significantly due to similar volumetric efficiencies between the fuels. The reduction in load range for these fuels is due to a large increase in the light load limit. Figure 9 indicates this is due to E30 and RD5-87 reaching the minimum allowable combustion efficiency levels at higher loads, indicating these fuels have poorer combustion efficiency at a given load level.

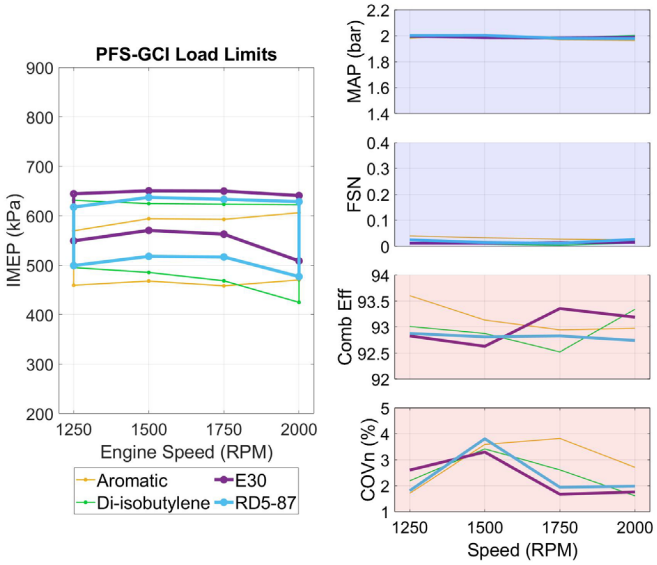

Figure 9. RD5-87 and E30 fuel load limits and load limit criteria.

The final two fuels, iso-octane and the cycloalkane, are added in Figure 10 and show further reductions in the working load range. As with the four prior fuels, Figure 10 shows high load is boost-limited. Similarly, the further reduction in operability is again due to the decreased combustion efficiency levels for the iso-octane and cycloalkane fuels. Like the four prior fuels at high load PFS-GCI conditions, the smoke emission levels for these two fuels are near-zero. Clearly, unlike SACI, smoke shouldn't be considered a limiting factor for PFS-GCI operation. A more important takeaway is that the total operability for PFS-GCI is significantly more sensitive to fuel chemistry than for SACI.

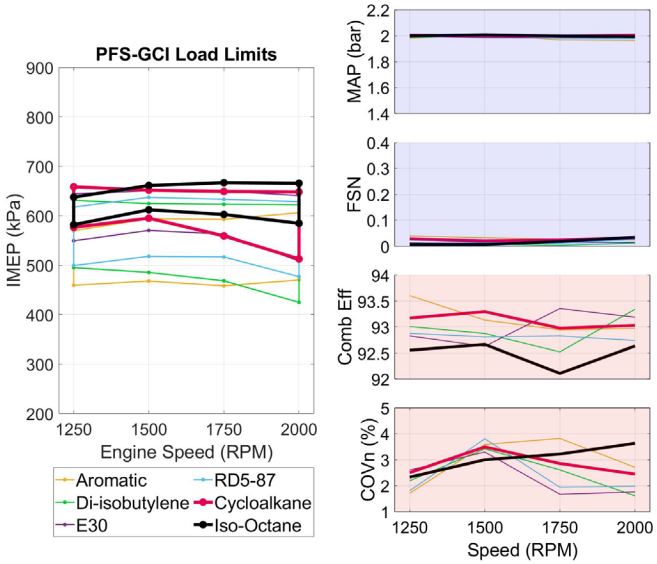

Figure 10. Cycloalkane and iso-octane fuel load limits and load limit criteria.

Fuel Chemistry Effects on ACI Heat Release

Heat release rates at 1250 RPM for high-load SACI operation with the cycloalkane, di-isobutylene, E30, and iso-octane fuels seen in Figure 11 show large differences between the fuels. Due to these heat release profiles being taken at the high load limit, the peak pressure rise rate for each case is at the maximum 7 bar/°CA. Thus, fuels prone to autoignition at lower pressures and temperatures, like iso-octane have to be phased later than a lower reactivity fuel like E30 to reduce the maximum pressure rise rate. This is reflected in the lower cylinder pressure (Figure 11) at the time of autoignition for iso-octane in comparison to E30 and the cycloalkane fuels. Effectively, differences in the combustion phasing indicate fuel-specific autoignition differences for SACI operation. Given this, E30 and cycloalkane are the fuels most resistant to auto-ignition, followed by di-isobutylene, and iso-octane is the fuel most prone to autoignition. The 1250 RPM high-load SACI points most likely lie in a temperature-pressure region where low temperature heat release (LTHR) is a significant contributing factor to autoignition, based on conclusions from prior work by Powell et al. [18]. This would explain the higher reactivity of iso-octane relative to the E30, cycloalkane, and di-isobutylene fuels.

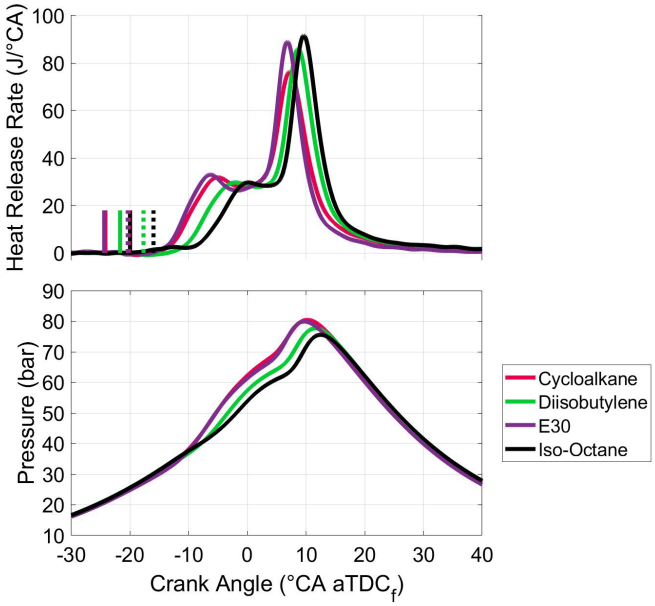

Figure 11. Heat release rates and pressure for cycloalkane, di-isobutylene, E30, and iso-octane under 1250 RPM, high-load SACI operation. Solid vertical lines prior to heat release indicate 2nd injection event, and dashed vertical lines indicate spark timing.

The cylinder pressure and heat release for RD5-87 and the aromatic fuel in Figure 12 reveal lower levels than the other 4 fuels due to the more smoke-limited peak load limits they could reach. As a result, no definitive fuel reactivity comparison can be made with the other four fuels.

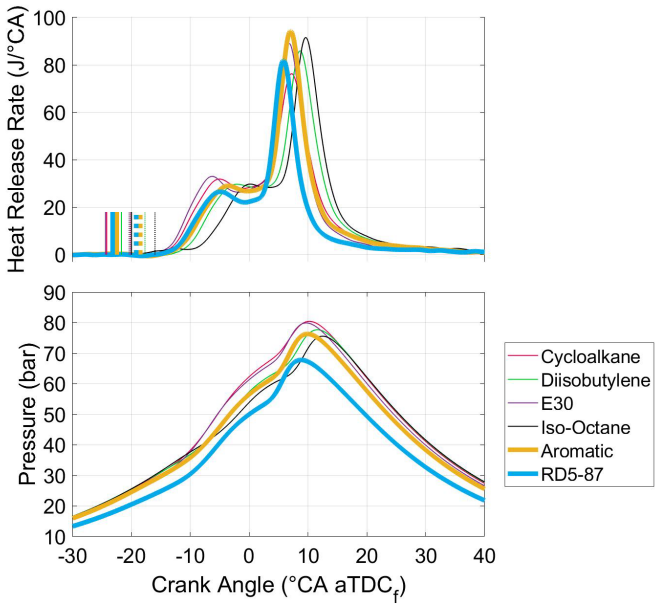

Figure 12. Pressure and heat release rates for aromatic and RD5-87 fuels compared with the other four fuels under 1250 RPM, high-load SACI operation

High load PFS-GCI operation at 1250 RPM starkly contrasts with SACI operation in Figure 13, due to the reduced fuel-chemistry related differences in cylinder pressure and heat release. While the fuel chemistry effects are more difficult to see, they are still present. Due to all high load PFS-GCI operation having been conducted at an intake pressure of 200 kPa, cylinder pressure at the time of autoignition is related to the effective compression ratio and fuel reactivity. More reactive fuels autoignite at lower pressure levels, thus the order of fuel reactivity is: 1) RD5-87 2) aromatic 3) di-isobutylene 4) iso-octane 5) E30 and 6) cycloalkane. These fuel autoignition resistance results are similar to those obtained by Powell et al. [18], suggesting similarly beyond-RON operation for PFS-GCI combustion here.

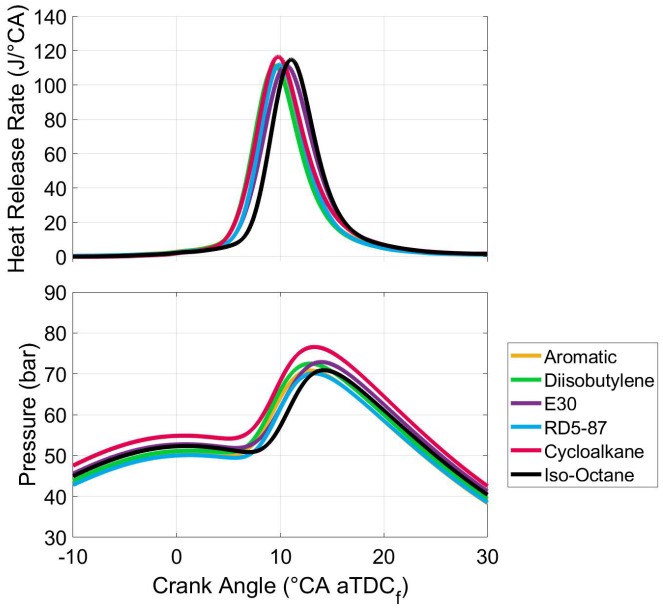

Figure 13. Pressure and heat release rates for all six fuels under 1250 RPM, high load PFS-GCI operation.

Change in ACI Combustion Response to Speed due to Fuel Chemistry

Additional speed effects as a function of fuel chemistry on ACI heat release rates were also observed. This behavior is examined in greater detail in this section by focusing on two fuels: iso-octane, which exhibits a significant amount of LTHR, and di-isobutylene, which does no exhibit significantly lower LTHR. These fuels were chosen because of their similar chemical structure, LHV, HoV, and stoichiometric air-fuel ratio.

Prior work by the authors on SACI operation [18] showed the importance of LTHR and pre-spark heat release (PSHR) as precursors to bulk autoignition. Figure 14 shows the impact of engine speed on heat release and cylinder pressure for iso-octane. One of the most evident features of the heat release rate is the presence of pre-spark heat release (PSHR) at 1250 RPM, a detailed view of this is shown in Figure 15. Notably, this PSHR event become negligible when the engine speed is increased to 1500 RPM. This is due to an increase in the exhaust and IVC temperatures and decrease in the available time for LTHR reactions with increasing speed [32]. The increase in compression temperatures with speed causes the pressure-sensitive LTHR chemistry to occur in the ideal 760-880K range earlier and a lower pressure, attenuating LTHR heat release [32]. There is also a notable decrease in the post-autoignition heat release rate in Figure 15 with increasing engine speed, reducing from a peak of 92 J/deg at 1250 RPM to 63 J/deg at 2000 RPM. However, the peak deflagration intensity doesn't change with speed.

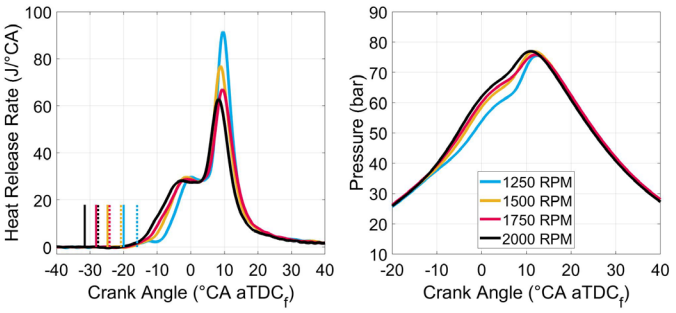

Figure 14. Heat release and cylinder pressure for SACI with iso-octane.

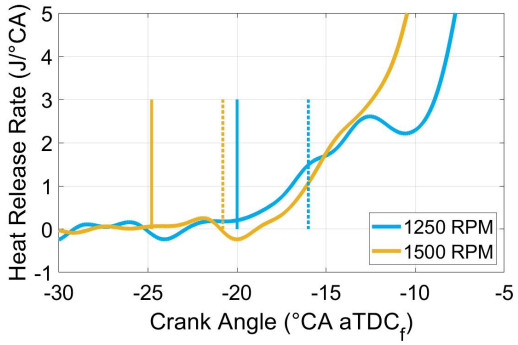

Figure 15. Detail of Pre-Spark Heat Release event at 1250 RPM, solid vertical lines indicate timing of 2nd injection and dashed vertical lines show the spark timing.

Figure 16 shows the heat release rate as a function of the mass fraction burned, where autoigniting fuel mass fraction is observed to decrease with engine speed. As a result, the total heat released by the deflagration event increases from ~25% to ~34%. Again, this is likely caused by a reduction in LTHR heat release with increasing engine speed. A direct result of this behavior is the end gas becomes increasingly dependent on the compressive heating from the deflagration event to reach the required conditions for autoignition.

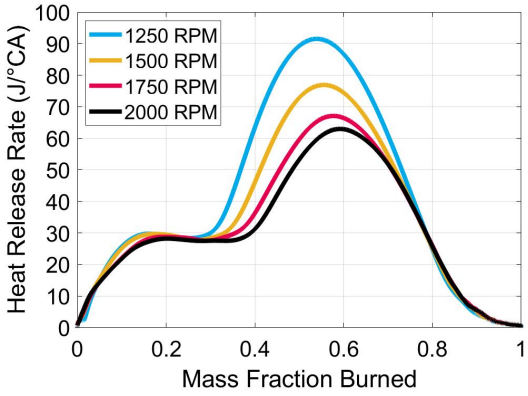

Figure 16. Reduction in SACI autoigniting mass fraction at the high-load limit using iso-octane with increasing engine speed.

Examining the SACI heat release for di-isobutylene, shown in Figure 17, there are notable deviations in behavior compared to iso-octane. The largest difference is the attenuated decrease in the peak post-autoignition heat release rate with speed. While the peak decreased by 29 J/deg for iso-octane, the decrease is 19 J/deg for di-isobutylene. Secondly, the di-isobutylene fuel doesn't display PSHR at 1250 RPM, despite operating under similar conditions.

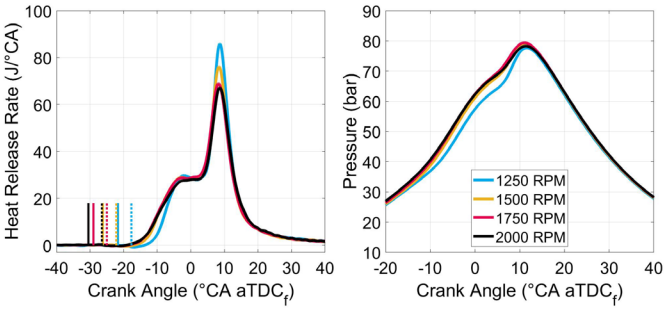

Figure 17. Heat release and cylinder pressure for SACI with the di-isobutylene fuel.

In a further departure from SACI operation with iso-octane, the autoigniting mass fraction did not change as significantly after 1500 RPM. This indicates that the energy contribution from the deflagration event is roughly fixed after 1500 RPM. The insensitivity of the end-gas autoignition to speed effects with di-isobutylene is due to a lack of changing end gas conditions brought about by LTHR at greater speeds.

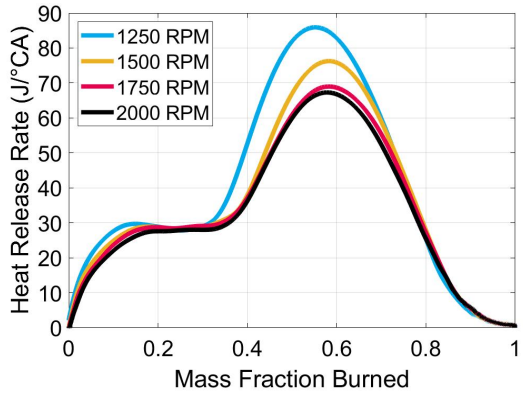

Figure 18. Fixed autoigniting SACI mass fraction above 1500 RPM for high-load SACI operation with the di-isobutylene fuel.

The PFS-GCI heat release and cylinder pressure for iso-octane from 1250 to 2000 RPM are shown in Figure 19. When examining the heat release, there is a notable decrease in peak rate, from 115 J/deg to 86 J/deg when increasing speed from 1250 to 2000 RPM. This accounts for a 26% drop in the maximum rate of heat release. While the magnitude of this is similar to that of SACI, the total percent reduction for SACI with iso-octane was higher at 33%.

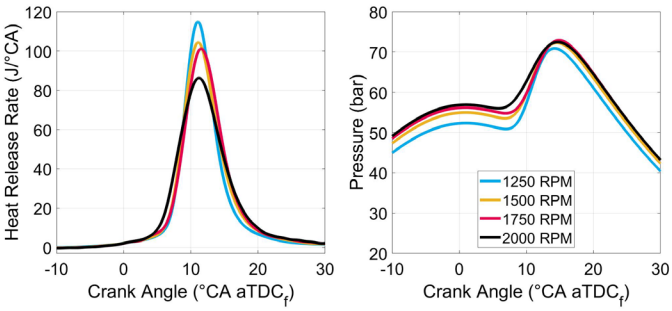

Figure 19. Heat Release and Pressure for PFS-GCI combustion with iso-octane.

The heat release rates and cylinder pressure for PFS-GCI operation over the 1250 to 2000 RPM speed range with the di-isobutylene fuel can be seen in Figure 20. Unlike with iso-octane, the peak heat release rate remains nearly constant for speeds of 1500 RPM and higher. The drop in peak heat release from 1250 to 1500 RPM is only 9 J/°CA, this only represents an 8% decrease. In contrast, the decrease for SACI operation with the di-isobutylene fuel was 19 J/°CA, constituting a 22% drop in peak heat release. Given these findings, the peak heat release rate is more sensitive to changes in engine speed for SACI combustion, regardless of the fuel chemistry.

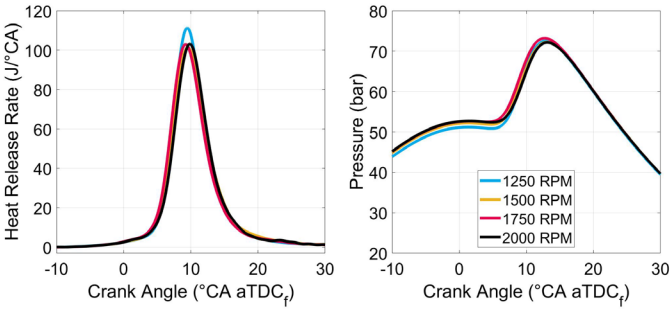

Figure 20. Heat Release and Pressure for PFS-GCI combustion with di-isobutylene fuel.

The effect of speed on decreasing the PFS-GCI heat release is more significant for iso-octane (Figure 19) than it is for the di-isobutylene fuel (Figure 20). Additional insight into this behavior is given by the intake valve closing timings required at the high load limit for each fuel in Figure 21. The steady advance in IVC timing for iso-octane indicates a greater required effective compression ratio in order to reach conditions favorable to autoignition. Contrastingly, the steady IVC requirement for the di-isobutylene fuel indicates a fixed effective compression ratio requirement. However, the slight retard in IVC timing with both fuels at 2000 RPM can't be explained by differences in intake pressure or exhaust temperature. The increasing effective compression ratio requirement suggests iso-octane is less reactive at higher speeds, while di-isobutylene has a more stable fuel reactivity with engine speed. This behavior is consistent with a decrease in the LTHR activity for iso-octane at higher speeds, leading to higher effective compression requirements. This change in iso-octane's reactivity with increasing speed is similar to the behavior observed with SACI.

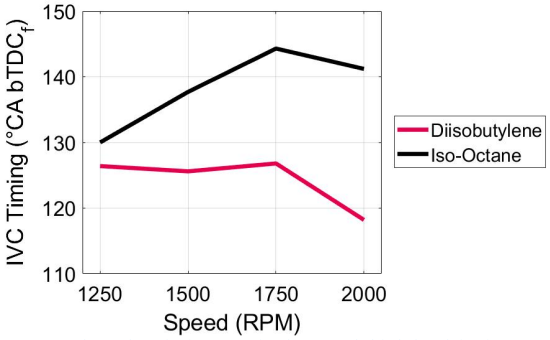

Figure 21. Intake valve timing required to reach high load for iso-octane and di-isobutylene fuels.

Discussion

This investigation sought to explore the fuel chemistry effects on the load limits for two ACI strategies in the context of multi-mode gasoline operation. As a result, design parameters such as the 12.5:1 compression ratio represent tradeoffs between ACI and SI operation. Similarly, the operating parameters for both ACI modes were chosen with the intent of showing fuel-specific differences on operability. Thus, full optimization for each fuel for the SACI and PFS-GCI operating modes were outside the scope. In contrast, Hu et al. [27] found similar SACI load limits using charge stratification, between 2 and 8 bar net IMEP, suggesting the SACI load limits measured in this investigation are in line with the available literature.

Given the operating methodology and load limit criteria laid out in the Experimental Setup and Procedure section, SACI was found to have a significantly higher load range than PFS-GCI. Additionally, some trends were discovered while exploring the load limits of PFS-GCI and SACI combustion modes. Generally, load-limits for SACI operation were found to be insensitive to the fuels investigated here, while they varied strongly for PFS-GCI.

It was found that intake boosting and injected fuel energy were predominantly the limiting factors for high load operation with both ACI modes. However, the high load limit and achievable load range for SACI, shown for 1500 RPM in Figure 22, was reduced considerably due to excessive smoke emissions for two high-PMI fuels. These two fuels were RD5-87 and the 98 RON aromatic, having PMI values of 1.71 and 1.80, respectively. Light load for

SACI was found to be mainly limited by combustion efficiency. The one exception to this was the aromatic fuel, which was limited by high cyclic variability. Despite this, five of the fuels tested shared the same SACI light load limits. Unusually, iso-octane required a higher minimum load to reach similar levels of combustion efficiency as the other fuels. Figure 22 shows the result is a 1500 RPM load range closer to the smoke-limited RD5-87 and aromatic fuels. This outlier behavior is possibly due to fuel properties and spray dynamics affecting the stratification levels at the time of combustion.

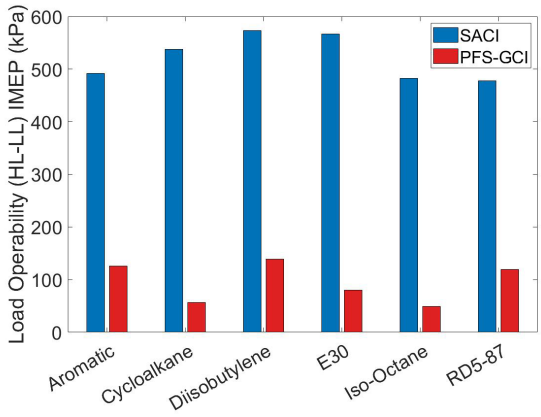

Figure 22. Load range, defined as high load minus low load, achieved for all six fuels under PFS-GCI and SACI operation at 1500 RPM.

The load range for PFS-GCI was found to vary strongly due to the fuel-specific differences in combustion efficiency at light loads, whereas the high-load limits changed less due to the methodology used in this study, where the peak intake manifold pressure encountered by all of the fuels in this study. The low-load limit is particularly characterized by the difference between the di-isobutylene and iso-octane fuels in Figure 22. At 1500 RPM, di-isobutylene has almost 3 times the load range of iso-octane, despite having almost identical high-load limits limited by intake boosting. Examining the results in Figure 22, iso-octane had reduced operability for both combustion modes due to its low combustion efficiency, making it a poor choice for ACI operation. On the other hand, the 98 RON di-isobutylene fuel had the highest load range at 1500 RPM due to its higher combustion efficiency and reduced operating smoke levels.

Given that the first four fuels in Figure 22 (Aromatic, Cycloalkane, Diisobutylene, and E30) all have the same nominal RON and S_{octane}, it is readily apparent that the ACI load limits can't be reliably attributed to any individual fuel properties. To further illustrate this, the 92 RON RD5-87, has almost the same load range for SACI as iso-octane, and as the 98 RON aromatic fuel for PFS. Similarly, the aromatic, cycloalkane, and E30 fuels all have S_{octane} values of nominally 10.5, yet have slightly different SACI and highly different PFS-GCI load ranges. The variation in load range with these properties varies by ACI mode, with PFS-GCI having the strongest deviations.

While excessive smoke emissions were an issue with SACI at high load, Figure 7 showed the inconsistency in the ability of fuel PMI to predict whether a fuel would be smoke limited at high load. Other studies have similarly highlighted the inconsistent ability of fuel PMI to predict particulate emissions [33]. Smoke emissions for the di-isobutylene fuel was nearly 0.4 FSN higher than the cycloalkane fuel, despite having a fuel PMI over three times lower (0.42 vs. 1.49). We hypothesize that the stratified charge used in SACI provides a greater opportunity for factors effecting mixture preparation to play a large role in soot formation, and in particular spray dynamics and fuel vaporization.

Summary/Conclusions

This investigation sought to explore the effects of fuel chemistry on the load operability of two ACI modes, SACI and PFS-GCI, over a speed range of 1250 to 2000 RPM. The fuels matrix included three 98 RON Co-Optima core fuels, a 98 RON fuel with di-isobutylene, RD5-87, and neat iso-octane.

1. SACI operability limits with the six fuels was higher than that of PFS-GCI, but fuel chemistry more strongly affected the load-operability levels for PFS-GCI.
2. High load for SACI and PFS-GCI was mainly found to be limited by intake boosting and trapped fuel mass, though fuels with PMI levels >1.7 were limited by smoke emissions approaching 1.0 FSN at high load during SACI operation.
3. ACI light load was found to depend strongly on combustion efficiency, which only varied slightly for SACI operation, but strongly for PFS-GCI operation.
4. Smoke emissions for SACI increased in a very non-linear fashion, likely due to rapidly increasing stratification levels and fuel pooling on the piston at high load. Contrasting smoke levels from PFS-GCI operation were negligible.
5. No traditional fuel properties were useful in predicting SACI or PFS-GCI load limits within the fuel set investigated here. RD5-87 had similar load limits to iso-octane for SACI and the 98 RON aromatic for PFS-GCI. Prediction of engine-out smoke emissions by fuel PMI is inconsistent, with the 98 RON di-isobutylene fuel producing more smoke than the 98 RON cycloalkane fuel, despite having a significantly lower PMI rating (0.42 versus 1.49). While combustion efficiency limits low-load operation, it can't be known apriori from fuel chemistry or fuel properties.
6. Engine speed affects ACI autoignition timing and heat release for low and high octane sensitivity fuels differently. iso-octane (low S_{octane}) exhibited large changes in ACI autoignition timing and heat release while the di-isobutylene fuel (high S_{octane}) exhibited minimal changes. These results are consistent with LTHR being the main autoignition driver for PFS-GCI and SACI, despite not being visible in the heat release data.

References

1. Scott, S., "Estimation of the Fuel Efficiency Potential of Six Gasoline Blendstocks Identified by the U.S. Department of Energy's Co-Optimization of Fuels and Engines Program," *SAE Technical Paper 2019-01-0017* 1–12, 2019, doi:10.4271/2019-01-0017.

2. Thring, R.H., "Homogeneous-Charge Compression-Ignition (HCCI) Engines," *SAE Technical Paper 892068* 1–9, 1989.

3. Heywood J.B, "Internal Combustion Engine Fundamentals," McGraw-Hill Inc., New York, ISBN 007028637X, 1988.

4. Chang, J., Güralp, O., Filipi, Z., Assanis, D.N., Kuo, T., Najt, P., and Rask, R., "New Heat Transfer Correlation for an HCCI Engine Derived from Measurements of Instantaneous Surface Heat Flux," *SAE Technical Paper*

2004-01-2996 1–18, 2004, doi:10.4271/2004-01-2996.

5. Caton, J.A., "A comparison of lean operation and exhaust gas recirculation: Thermodynamic reasons for the increases of efficiency," *SAE Technical Paper 2013-01-0266*, 2013, doi:10.4271/2013-01-0266.

6. Lawler, B., Ortiz-Soto, E., Gupta, R., Peng, H., and Filipi, Z.S., "Hybrid Electric Vehicle Powertrain and Control Strategy Optimization to Maximize the Synergy with a Gasoline HCCI Engine," *SAE Int. J. Engines* 4(1):1115–1126, 2011, doi:10.4271/2011-01-0888.

7. Zyada, A., Hollowell, J., Shirley, M., Fantin, N., Zhu, S., Roh Joo, N., and Zoldak, P., "Demonstration of Better than Diesel Efficiency and Soot Emissions using Gasoline Compression Ignition in a Light Duty Engine with a Fuel Pressure Limitation," *SAE Technical Paper 2021-01-0518*, 2021.

8. Dempsey, A., Curran, S., and Wagner, R., "A perspective on the range of gasoline compression ignition combustion strategies for high engine efficiency and low NOx and soot emissions: Effects of in-cylinder fuel stratification," *Int. J. Engine Res.* 17(8):897–917, 2016, doi:10.1177/1468087415621805.

9. Eng, J.A., "Characterization of Pressure Waves in HCCI Combustion," *SAE Technical Paper 2002-01-2859*, 2002, doi:10.4271/2002-01-2859.

10. Curran, S. and Wagner, R., "Impact of Multimode Range and Location on Urban Fuel Economy on a Light-Duty Spark-Ignition Based Powertrain Using Vehicle System Simulations," *SAE Technical Paper 2020-01-1018*, 2020, doi:10.4271/2020-01-1018.

11. Szybist, J.P., Nafziger, E., and Weall, A., "Load expansion of stoichiometric HCCI using spark assist and hydraulic valve actuation," *SAE Int. J. Engines* 3(2):244–258, 2010, doi:10.4271/2010-01-2172.

12. Olesky, L.M., Martz, J.B., Lavoie, G.A., Vavra, J., Assanis, D.N., and Babajimopoulos, A., "The effects of spark timing, unburned gas temperature, and negative valve overlap on the rates of stoichiometric spark assisted compression ignition combustion," *Appl. Energy* 105:407–417, 2013, doi:10.1016/j.apenergy.2013.01.038.

13. Yun, H., Wermuth, N., and Najt, P., "Extending the High Load Operating Limit of a Naturally-Aspirated Gasoline HCCI Combustion Engine," *SAE Int. J. Engines* 3(1):681–699, 2010, doi:10.4271/2010-01-0847.

14. Nakai, E., Goto, T., Ezumi, T., Twumura, Y., Endou, K., Kanda, Y., Urushihara, T., Sueoka, M., and Hitomi, M., "Mazda SKYACTIV-X 2.0L gaoline engine," *Proceedings of the 28th Aachen Colloqium Automobile and Engine Technology*, 55–78, 2019.

15. Szybist, J.P., Busch, S., McCormick, R.L., Pihl, J.A., Splitter, D.A., Ratcliff, M.A., Kolodziej, C.P., Storey, J.E., Moses-Debusk, M., Vuilleumier, D., Sjoberg, M., Sluder, C.S., Rockstroh, T., and Miles, P., "What Fuel Properties Enable Higher Thermal Efficiency in Spark-Ignited Engines?," *Prog. Energy Combust. Sci.* 82(100876), 2020.

16. Szybist, J.P. and Splitter, D.A., "Impact of Engine Pressure-Temperature Trajectory on Autoignition for Varying Fuel Properties," *Appl. Energy Combust. Sci.* 1–4(June):100003, 2020, doi:10.1016/j.jaecs.2020.100003.

17. Lopez Pintor, D., Dec, J., and Gentz, G., "φ-sensitivity for LTGC engines: Understanding the fundamentals and tailoring fuel blends to maximize this property," *SAE Technical Paper 2019-01-0961* 1–24, 2019, doi:10.4271/2019-01-0961.

18. Powell, T., Szybist, J., Dal Forno Chuahy, F., Curran, S., Mengwasser, J., Aradi, A., and Cracknell, R., "Octane Index Applicability over the Pressure - Temperature Domain," *Energies* 14(3):607, 2021.

19. Szybist, J.P. and Splitter, D.A., "Pressure and temperature effects on fuels with varying octane sensitivity at high load in SI engines," *Combust. Flame* 177:49–66, 2017, doi:10.1016/j.combustflame.2016.12.002.

20. Jatana, G.S., Splitter, D.A., Kaul, B., and Szybist, J.P., "Fuel property effects on low-speed pre-ignition," *Fuel* 230(May):474–482, 2018, doi:10.1016/j.fuel.2018.05.060.

21. Kalghatgi, G.T., "Fuel anti-knock quality-part I. Engine studies," *SAE Technical Paper 2001-01-3584*, 2001, doi:10.4271/2001-01-3584.

22. Kalghatgi, G.T., Nakata, K., and Mogi, K., "Octane Appetite Studies in Direct Injection Spark Ignition (DISI) Engines," *SAE Technical Paper 2005-01-0244* 1(April 2005), 2005, doi:10.4271/2005-01-0244.

23. Woschni, G. and Spindler, W., "Heat Transfer With Insulated Combustion Chamber Walls and Its Influence on the Performance of Diesel Engines," *J. Eng. Gas Turbines Power* 110(July 1988):482, 1988, doi:10.1115/1.3240146.

24. Ortiz-Soto, E., Vavra, J., and Babajimopoulos, A., "Assessment of Residual Mass Estimation Methods for Cylinder Pressure Heat Release Analysis of HCCI Engines With Negative Valve Overlap," *J. Eng. Gas Turbines Power* 134(8):082802, 2012, doi:10.1115/1.4006701.

25. Yun, H.J. and Mirsky, W., "Schlieren-Streak Measurements of Instantaneous Exhaust Gas Velocities from a Spark-Ignition Engine," *SAE Technical Paper 741015*, 1974.

26. Fitzgerald, R.P., Steeper, R., Snyder, J., Hanson, R., and Hessel, R., "Determination of Cycle Temperatures and Residual Gas Fraction for HCCI Negative Valve Overlap Operation," *SAE Int. J. Engines* 3(1):2010-01–0343, 2010, doi:10.4271/2010-01-0343.

27. Hu, Z., Zhang, J., Sjöberg, M., and Zeng, W., "The use of partial fuel stratification to enable stable ultra-lean deflagration-based Spark-Ignition engine operation with controlled end-gas autoignition of gasoline and E85," *Int. J.*

Engine Res. 21(9):1678–1695, 2020, doi:10.1177/1468087419889702.

28. Fouts, L.A., Fioroni, G.M., Christensen, E.D., Ratcliff, M.A., McCormick, R.L., Zigler, B.T., Sluder, S., Szybist, J.P., Dec, J.E., Miles, P.C., Ciatti, S., Bays, J.T., Pitz, W., and Mehl, M., "Co-Optimization of Fuels & Engines: Properties of Co-Optima Core Research Gasolines. Technical Report NREL/TP-5400-71341," Golden, CO: National Renewable Energy Laboratory, 2018, doi:10.2172/1467176.

29. Gentz, G., Dernotte, J., Ji, C., Lopez Pintor, D., and Dec, J., "Combustion-Timing control of Low-Temperature gasoline combustion (LTGC) engines by using double Direct-Injections to control kinetic rates," *SAE Technical Paper 2019-01-1156*, 2019, doi:10.4271/2019-01-1156.

30. Pintor, D.L., Dec, J., and Gentz, G., "Experimental Evaluation of a Custom Gasoline-Like Blend Designed to Simultaneously Improve ϕ -Sensitivity, RON and Octane Sensitivity," *SAE Int. J. Adv. Curr. Pract. Mobil.* 2(4):2196–2216, 2020, doi:10.4271/2020-01-1136.

31. Aikawa, K., Sakurai, T., and Jetter, J.J., "Development of a predictive model for gasoline vehicle particulate matter emissions," *SAE Int. J. Fuels Lubr.* 3(2):610–622, 2010, doi:10.4271/2010-01-2115.

32. Sjöberg, M. and Dec, J.E., "EGR and intake boost for managing HCCI low-temperature heat release over wide ranges of engine speed," *SAE Technical Paper 2007-01-0051*, 2007, doi:10.4271/2007-01-0051.

33. Kim, N., Vuilleumier, D., He, X., and Sjöberg, M., "Ability of Particulate Matter Index to describe sooting tendency of various gasoline formulations in a stratified-charge spark-ignition engine," *Proc. Combust. Inst.* 38(4):1–9, 2021, doi:10.1016/j.proci.2020.06.173.

Contact Information

The corresponding author can be contacted at szybistjp@ornl.gov.

Funding

This research was funded by the U.S. Department of Energy (DOE) Office of Energy Efficiency and Renewable Energy (EERE) as part

Acknowledgments

This research was conducted as part of the Co-Optima Initiative sponsored by the U.S. DOE EERE, Bioenergy Technologies and Vehicle Technologies Offices. Co-Optima is a collaborative Initiative of multiple National Laboratories initiated to simultaneously accelerate the introduction of affordable, scalable, and sustainable biofuels and high-efficiency, low-emission vehicle engines. A special thanks to Kevin Stork, Gurpreet Singh, and Mike Weismiller.

We would like to thank Flavio Chuahy at ORNL for helping to establish the methodology for the SACI and PFS-GCI strategies.

We would also like to thank GM for their engine hardware support, particularly Arun Solomon and Paul Najt.

Disclaimer

Definitions/Abbreviations

°CA - Degrees crank angle

ACI - Advanced compression ignition

aTDC$_f$ - degrees after top dead center

bTDC$_f$ - degrees after top dead center

COV - coefficient of variation

DI - direct injection

E10 - 10% ethanol

FBP - full boiling point

FSN - filter smoke number

HFS – heavy fuel stratification

IMEP - indicated mean effective pressure

IMEPg - gross indicated mean effective pressure

LTHR - low temperature heat release

NO_x - oxides of nitrogen

PFS – partial fuel stratification

PFS-GCI - partial fuel stratification – gasoline compression ignition

PMI - particulate matter index

PPCI – partially premixed compression ignition

PPRR - peak pressure rise rate

PSHR - pre-spark heat release

RCCI - reactivity-controlled compression ignition

RON - research octane number

RPM - revolutions per minute

SACI - spark-assisted compression ignition

SI - spark ignition

S_{octane} - octane sensitivity

TDC - top dead center

φ - equivalence ratio